
INCEPTION-AUGMENTATION GENERATIVE ADVERSARIAL NETWORK

A PREPRINT

Saman Motamed^{1,2} and Farzad Khalvati^{1,2}

¹Department of Medical Imaging, University of Toronto

²The Hospital for Sick Children, Toronto, ON, Canada

April 22, 2022

ABSTRACT

Successful training of convolutional neural networks (CNNs) requires a substantial amount of data. With small datasets, networks generalize poorly. Data Augmentation techniques improve the generalizability of neural networks by using existing training data more effectively. Standard data augmentation methods, however, produce limited plausible alternative data. Generative Adversarial Networks (GANs) have been utilized to generate new data and improve CNN performance. Nevertheless, generative models have not been used for augmenting data to improve the training of another generative model. In this work, we propose a new GAN architecture for semi-supervised augmentation of chest X-rays for the detection of pneumonia. We show that the proposed GAN can augment data for a specific class of images (pneumonia) using images from both classes (pneumonia and normal) in an image domain (chest X-rays). We demonstrate that using our proposed GAN-based data augmentation method significantly improves the performance of the state-of-the-art anomaly detection architecture, AnoGAN, in detecting pneumonia in chest X-rays, increasing AUC from 0.83 to 0.88.

1 Introduction

In recent years, Convolutional Neural Networks (CNNs) have shown excellent results on several tasks, given sufficient data [5, 6, 9]. One of the main reasons for poor CNN performance and overfitting on training data remains limited-sized datasets in many domains such as medical imaging. Improving the performance of CNNs can be achieved by using the existing data more effectively. Augmentation methods such as random rotations, flips, and adding various noise profiles have been proposed [4, 20] as some methods of augmentation. Typical data augmentation techniques use a limited series of invariances that are easy to compute and therefore are limited in the amount of new data they can generate.

Generative Adversarial Networks (GANs) [3] have been used for data augmentation to improve training CNNs by generating new data without any pre-determined augmentation method. Cycle-GAN was used to generate synthetic non-contrast CT images by learning the transformation of contrast to non-contrast CT images [14]. This improved results in CT segmentation using a U-Net model [12]. Using Deep Convolutional-GAN (DCGAN) [11] and Conditional-GAN [10] to augment medical CT images of liver lesion and mammograms showed improved results in classification of lesions using CNNs [2, 18]. Data Augmentation GAN (DAGAN) [1] was able to improve the performance of vanilla

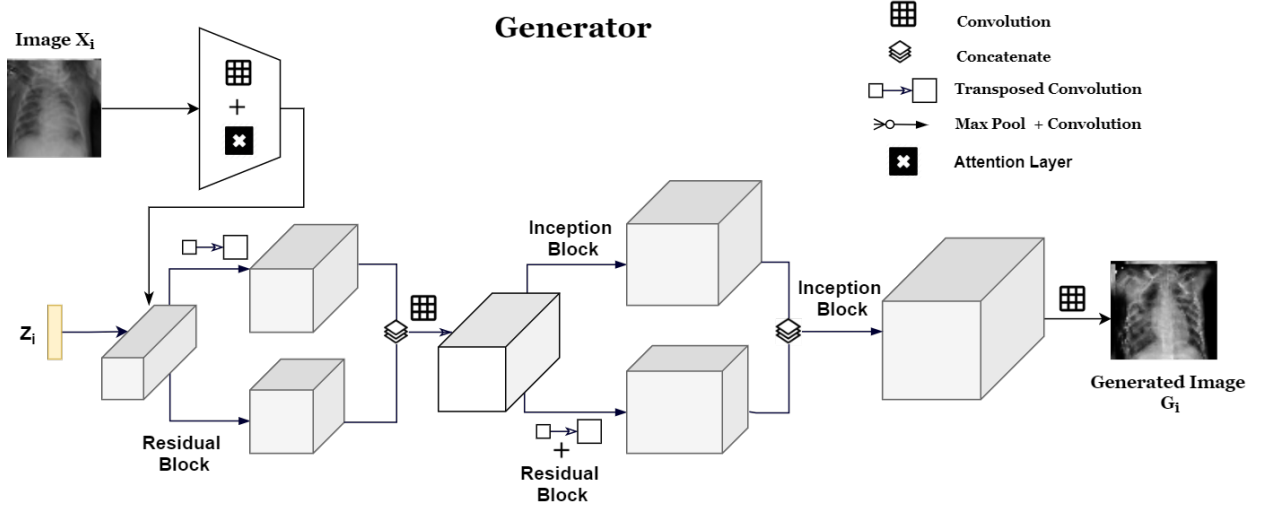


Figure 1: IAGAN’s Generator Architecture

CNN classifiers on EMNIST, VGG-Face and Omniglot datasets by training DAGAN in a source domain and generating new data from the target domain. There has not been any study on data augmentation using GANs for training other GANs. The challenge with using a GAN to augment data for training another GAN is for a trained GAN how to learn the true distribution of training images. Newly generated images with the trained generator of the GAN follow the same distribution, and hence there is nothing new to be learned by another GAN that trains on the original images combined with the newly generated images.

In this paper, we propose a novel Inception-Augmentation GAN (IAGAN) model inspired by DAGAN [1] for the task of data augmentation that specifically improves the performance of another GAN architecture. We train our IAGAN on chest X-rays with pneumonia from a dataset containing normal and pneumonia cases. We demonstrate that a trained IAGAN can generate new X-ray images using both pneumonia and normal images in order to augment pneumonia dataset. We evaluate the performance of IAGAN by training a convolutional GAN for anomaly detection (AnoGAN) [15] and show improved results in classifying pneumonia and normal cases with an 5% increase in the area under the receiver operating characteristic (ROC) curve (AUC). We also show our trained IAGAN is able to generate new domain specific data regardless of the class of its input images. This allows for an semi-supervised data augmentation in the case of not having labels for a subset of the dataset.

2 IAGAN Architecture

Figure 1 shows the architecture of the proposed IAGAN’s Generator. DAGAN [1] introduces the idea of the secondary input to the generator but they do not discuss the architecture details and how they use the second image. We use the idea of a secondary input image in our IAGAN’s generator architecture. At each iteration i , the generator (G) takes as input a Gaussian noise vector z_i and real image x_i . To achieve a more accurate representation of the input image x_i , we encode it using convolution and attention layers to a lower-dimensional representation of image x_i before being concatenated with projected noise vector z_i . This dual input to the generator allows the trained generator to later on use images from different classes and generate a broader range of images to augment our specific training data class. The use of Attention layers in GANs (Figure 2) has shown to capture long-range dependencies in the image [19] where simple convolution layers focus on local features restricted by their receptive field, self-attention layers capture a broader range of features within the image. The attention layer uses three 1×1 convolutions. 1×1 convolution helps reduce the number of channels in the network. Two of the convolution outputs, as suggested in Figure 2 are multiplied (matrix multiplication) and fed to a *softmax* activation, which results in producing the attention map. The attention map

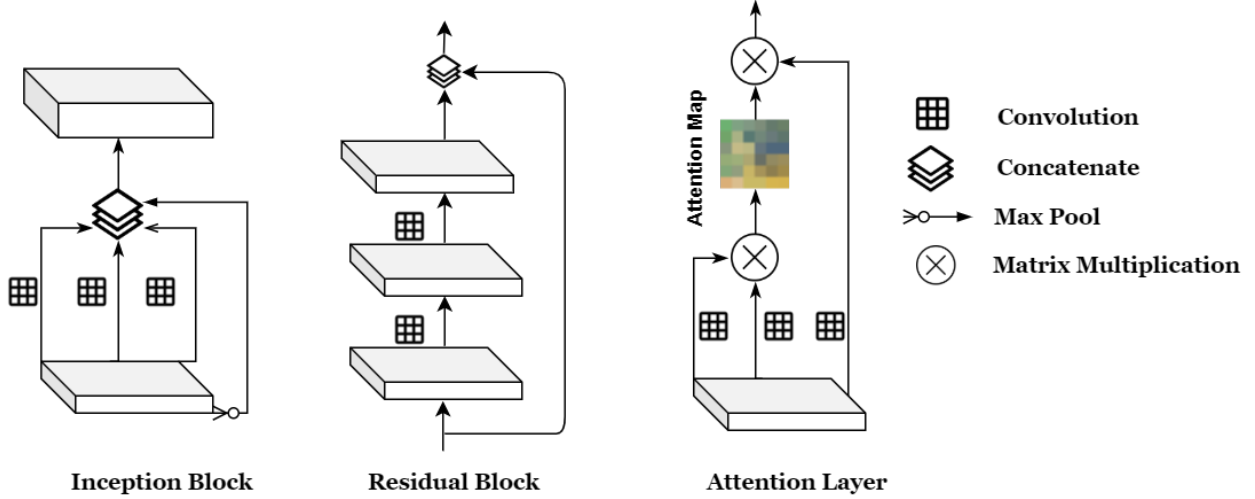


Figure 2: IAGAN’s Generator specific architecture breakdown

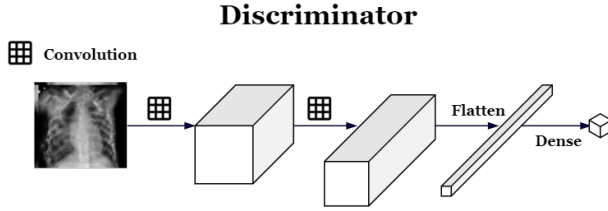


Figure 3: Discriminator Architecture

acts as the probability of each pixel affecting the output of the third convolution layer. Feeding a lower-dimensional representation of an input image x allows for the trained generator to use images from different classes to produce similar never-before-seen images of the class it was trained on.

Using Inception and residual architectures [16] increase GAN’s ability to capture more details from training image-space without losing spatial information after each convolution and pooling layer. Making the generator G deeper is theoretically a compelling way to capture more details in the image, but deep GANs are unstable and hard to train [8, 11]. A trained G learns the mapping $G(z) : z \mapsto x$ from latent space representations z to realistic, $2D$, chest X-ray images.

The discriminator (D) (Figure 3) is a 4-layer CNN that maps a 2D image to a scalar output that can be interpreted as the probability of the given input being a real chest X-ray image sampled from training data or image $G(z)$ generated by the generator G . Optimization of D and G can be thought of as the following game of minimax [3] with the value function $V(G, D)$:

$$\min_G \max_D V(D, G) = \mathbb{E}_{x \sim P_{data}(x)} [\log D(x)] + \mathbb{E}_{z \sim P_z(z)} [\log(1 - D(G(z)))] \quad (1)$$

During training, generator G is trained to minimize the accuracy of discriminator D ’s ability in distinguishing between real and generated images while the discriminator is trying to maximize the probability of assigning real training images the "real" and generated images from G , "fake" labels. During the training, G improves at generating more realistic images while D gets better at correctly identifying between real and generated images.

3 IAGAN Training and Data Generation

3.1 Dataset

We used the publicly available chest X-ray dataset [7] with two categories of Normal - 1,575 images and Pneumonia - 4,265 images. The images were in jpeg format and varied in size, with pixel values in $[0, 255]$ range. We resized all images to 64×64 pixels. Images were normalized to have $[-1, 1]$ range for tanh non-linearity activation in the IAGAN architecture. We use our bigger cohort (pneumonia) as the training class. We split pneumonia images into 3,265 training and 1,000 test images. To keep the test set balanced, we randomly chose 1,000 images of normal cases for a total of 3,265 training and 2,000 test images.

3.2 Training

IAGAN was trained on 3,265 chest X-rays with pneumonia. Mean squared error (MSE) was used as the loss function for both the generator and discriminator of IAGAN. The goal was that the trained IAGAN would generate new images that have a similar distribution to the images of training class c and, at the same time, the newly generated images would be dissimilar enough to the images of the training class so they can be used for augmentation of class c images. Feeding the down-sampled input image to the generator helps with this objective; however, to enforce the dissimilarity between real and generated images further, we used the structural similarity index (SSIM) measure [17]. At each iteration of G’s training, $SSIM(x_i, g(z_i))$ is calculated for the training image batch x_i and generated images $g(z_i)$. $SSIM$ values can vary between -1 and 1, where 1 indicates perfect similarity. We pass a weight of $1 - [(SSIM + 1)/2]$ to G’s loss update in order to promote a level of dissimilarity between generated images and training images.

Learning rates of 0.0004 and 0.0001 were used for the discriminator and generator, respectively. Experimenting with the size of the Gaussian noise vector z showed 125 to be the optimal size. We trained our IAGAN for 150 epochs on an Nvidia GeForce RTX 2080 Ti - 11 GB with a batch size of 16.

3.3 Generating New Data

When IAGAN is trained, the generator has learned the mapping $G(z) : z \mapsto x$ from latent space representation $G(z)$ to realistic images (chest X-ray with pneumonia). To generate a new image given a query image x as input to G, we want to find a point $G(z)$ from the latent space that given the generator’s output on that point, $G(z)$, falls under the same class as image x . The expected behaviour after successful training is that the query image x if affected by pneumonia, will result in finding an image $G(z)$ which lies in the same class that the generator has been trained on, but it looks different enough from x to be used to augment the training cohort.

To find an ideal latent variable $G(z)$, we used back-propagation with a predefined number of steps. The loss function defined to find such z through back-propagation was comprised of two components; *residual loss* and *discrimination loss*. Residual loss (\mathcal{L}_R) calculates the L1 distance between $G(z)$ and the query image x and enforces visual similarity between the query image and generated image.

$$\mathcal{L}_R(z_i) = \sum |x - G(z_i)| \quad (2)$$

Schlegl *et al.* [15] proposed a discrimination loss (\mathcal{L}_D) inspired by the concept of feature matching [13] that enforces generated images $G(z_i)$ to follow the statistical characteristics of the training images. (\mathcal{L}_D) is defined below where the output of an intermediate layer of the discriminator $f(\cdot)$ is used to represent the input image’s statistical characteristics.

$$\mathcal{L}_D(z_i) = \sum |f(x) - f(G(z_i))| \quad (3)$$

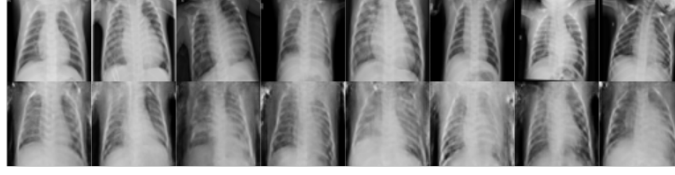


Figure 4: Original and Augmented Pneumonia Images; Top row images are original images identified with pneumonia and the corresponding augmented images are on the bottom row

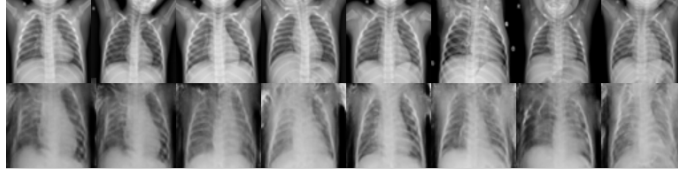


Figure 5: Original and Augmented Normal Images; Top row images are original images identified as normal and the corresponding augmented images are on the bottom row

The overall loss used to back-propagate and find the best z is a weighted sum of residual and discrimination loss;

$$\mathcal{L}(z_i) = (1 - \lambda) \times \mathcal{L}_R(z_i) + \lambda \times \mathcal{L}_D(z_i) \quad (4)$$

To generate new images, we set the back-propagation steps to 400 and use $\lambda = 0.7$. This choice of lambda puts more weight on enforcing statistical characteristics of the generated image over the visual similarity between training images and newly generated image $G(z)$ to help with generated data being used for augmentation.

For each pneumonia image from the training cohort, we generate an image using IAGAN’s trained Generator. This augmentation results in a training cohort of 6,530 original and augmented pneumonia images (Figure 4). We also augmented 575 normal images that were not used in testing the IAGAN’s performance. We use these normal images as input to trained IAGAN and generate 575 pneumonia cases from normal cases shown in Figure 5.

4 Evaluation

Schlegl *et al.* [15] proposed AnoGAN for detecting anomalies in optical coherence tomography images of the retina. The AnoGAN architecture follows DCGAN [11] in terms of overall generator and discriminator architecture. They train the AnoGAN model on one class of images. With the trained generator G at hand, in order to find anomalies in image x , back-propagation is used with the loss function of Equation 4 with $\lambda = 0.2$. Upon finding a point z after a set number of iterations (500 iterations in our experiments), the anomaly score $A(x)$ is defined using residual (Equation 2) and discrimination (Equation 3) losses as shown below where $R(z)$ is the residual loss for point z and $D(z)$ is the discrimination loss.

$$A(x) = (1 - \lambda) \times R(z) + \lambda \times D(z) \quad (5)$$

We trained AnoGAN on pneumonia images and calculated anomaly scores of test images. Higher anomaly scores correspond to healthy cases, whereas lower anomaly scores correspond to pneumonia images. Each instance of AnoGAN was trained for 100 epochs with a batch size of 16, with fixed hyper-parameters to compare the effects of augmentation using IAGAN’s generated images. We also used AnoGAN to perform the same type of augmentation to compare the results of our generative augmentation with another network.

AnoGAN training instances are as follows.

- AnoGAN trained on 3,265 real pneumonia images

- AnoGAN trained on 6,530 images: 3,265 real pneumonia images and 3,265 augmented images using another AnoGAN architecture. The same process with back-propagation was used with the difference that in AnoGAN there is no input image so the generator only takes in a random point z .
- AnoGAN trained on 7,105 images: 3,265 real pneumonia images and 3,840 images augmented using IAGAN with 575 normal and 3,265 pneumonia images as input.

5 Results

Anomaly scores (Equation 5) were computed for images in the test set (1,000 normal and 1,000 pneumonia). We plotted the ROC curve (Figure 6) for the three trained AnoGANs. The first AnoGAN was trained on 3,265 pneumonia images without any augmentation. The second AnoGAN was trained on 6,530 pneumonia images, half of which were generated using the first AnoGAN as data augmentation method. For each pneumonia training image, we found a similar image using the trained AnoGAN’s generator via back-propagation and Equation 4. This doubled the number of images from 3,265 to 6,530, which were used to train the second AnoGAN. The last (third) AnoGAN was trained using 7,105 images where 3,840 of the images have been generated using our trained IAGAN by feeding the network with 575 normal and 3,265 pneumonia labeled images. This generated 575 and 3,265 augmented images, both of pneumonia class, which were added to the original 3,256 training pneumonia data (total of 7,105). IAGAN augmentation improves AUC from 0.83 to 0.88. When augmenting pneumonia dataset using AnoGAN, the AUC drops by 1%.

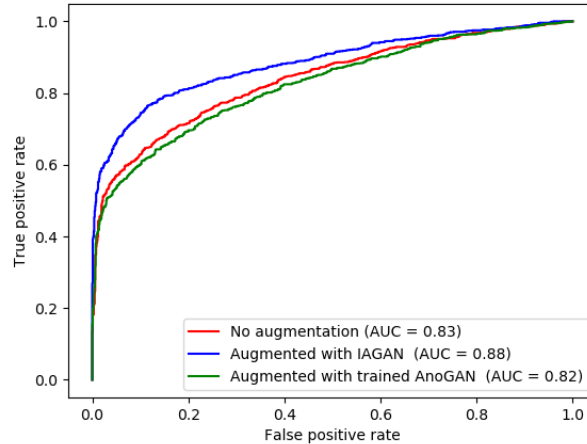


Figure 6: ROC curves of different instances of trained AnoGAN architecture on pneumonia images. One with no augmentation, one with augmentation using the same AnoGAN architecture and one augmentation using our IAGAN

The average anomaly score for 1,000 normal test images were: 604 for AnoGAN with no augmentation, 618 for augmented by AnoGAN, and 666 for augmented by IAGAN. For cases with pneumonia, the mean anomaly score was 473, 480, and 506 for AnoGAN with no augmentation, AnoGAN augmented by AnoGAN, and AnoGAN augmented by IAGAN, respectively. This shows that the anomaly score gap is larger in the IAGAN augmented instance (160 vs. 131 and 138). The larger gap indicates that the AnoGAN is more confident in classification of normal and pneumonia images when augmented with IAGAN. Figure 7 shows the bar chart for computed anomaly scores for normal and pneumonia test images.

To demonstrate the ability of IAGAN in using data from different classes within a domain to augment a specific class of images (i.e., using normal images to augment pneumonia class), we trained an AnoGAN on real pneumonia training images and tested the trained model on 1,150 images: 575 normal images that were not used in training and 575 IAGAN generated pneumonia images using the normal images. Treating the IAGAN generated images as pneumonia,

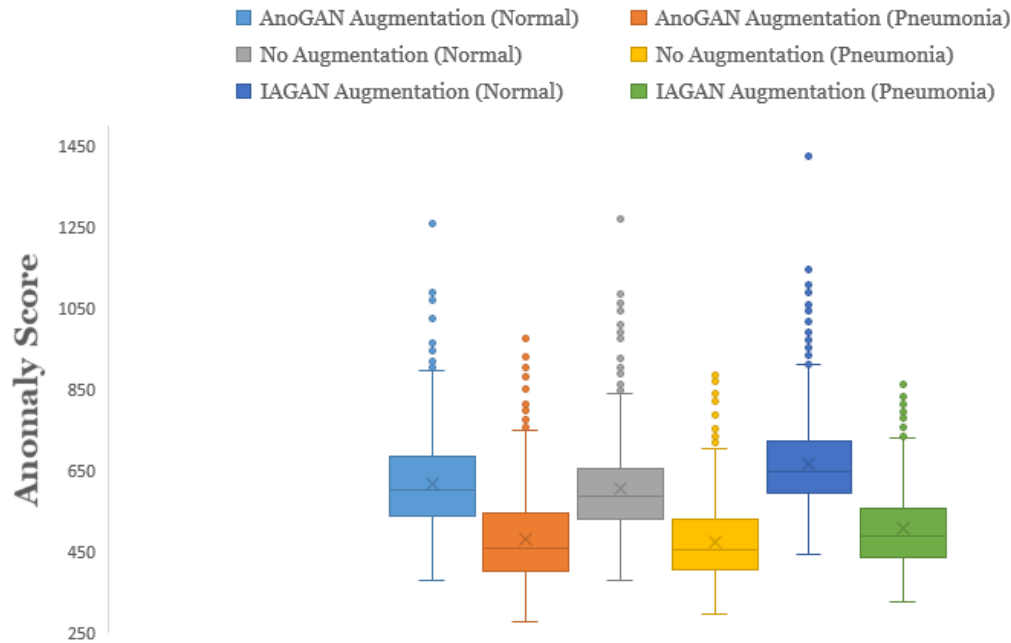


Figure 7: Computed anomaly score for the three training instances of AnoGAN with and without augmentation, separated into the class labels; normal and pneumonia.

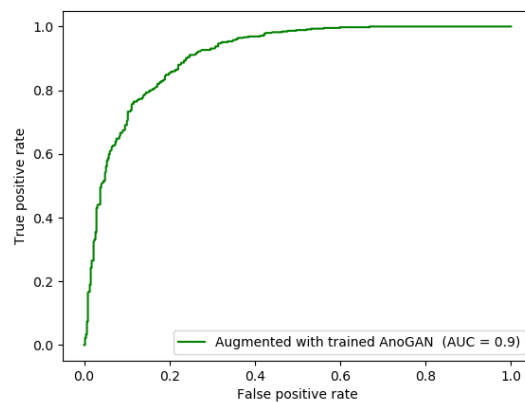


Figure 8: ROC plot for AnoGAN trained on real pneumonia cases and tested on normal cases turned into pneumonia using IAGAN.

we achieve an AUC of 0.9. This shows pneumonia augmented images using normal cases as input to IAGAN’s trained generator generated images that classify as pneumonia. Figure 8 shows the ROC curve of test images.

6 Conclusion

In this paper, we presented IAGAN; a semi-supervised GAN-based augmentation method. We showed that a traditional GAN with a single random noise vector input to the generator fails in augmenting data to train another generative model. Our proposed IAGAN architecture, however, shows substantial improvement when used for augmentation of the

training cohort. We used the AnoGAN [15] architecture to show a 5% improvement in AUC when training data was augmented using our proposed IAGAN.

IAGAN architecture allows for semi-supervised augmentation of data for a specific class of labels (pneumonia). We showed that by training IAGAN on a specific class (pneumonia), we were able to use data from both classes (normal and pneumonia) to augment pneumonia data. The semi-supervised augmentation ability allows IAGAN to use unlabelled data in a specific domain (chest X-rays) to generate new data for a specific class.

Broader Impact

Data bias in training neural networks can put minorities at risk when working with medical data, where data does not entail a balanced demographic. Medical images are no exception to this issue of bias in collecting datasets and training neural networks. With our work, the data of underrepresented population can be augmented using either the data of the mainstream population or a combination of both mainstream and minority population. This work can be used to balance datasets by augmenting the underrepresented class and potentially reducing the bias in medical imaging data.

References

- [1] Antreas Antoniou, Amos Storkey, and Harrison Edwards. Data augmentation generative adversarial networks. *arXiv preprint arXiv:1711.04340*, 2017.
- [2] Maayan Frid-Adar, Idit Diamant, Eyal Klang, Michal Amitai, Jacob Goldberger, and Hayit Greenspan. Gan-based synthetic medical image augmentation for increased cnn performance in liver lesion classification. *Neurocomputing*, 321:321–331, 2018.
- [3] Ian Goodfellow. Nips 2016 tutorial: Generative adversarial networks. *arXiv preprint arXiv:1701.00160*, 2016.
- [4] Ruqian Hao, Khashayar Namdar, Lin Liu, Masoom A. Haider, and Farzad Khalvati. A comprehensive study of data augmentation strategies for prostate cancer detection in diffusion-weighted mri using convolutional neural networks. *arXiv preprint arXiv:2006.01693*, 2020.
- [5] Kaiming He, Xiangyu Zhang, Shaoqing Ren, and Jian Sun. Delving deep into rectifiers: Surpassing human-level performance on imagenet classification. In *Proceedings of the IEEE international conference on computer vision*, pages 1026–1034, 2015.
- [6] Kaiming He, Xiangyu Zhang, Shaoqing Ren, and Jian Sun. Deep residual learning for image recognition. In *Proceedings of the IEEE conference on computer vision and pattern recognition*, pages 770–778, 2016.
- [7] Daniel Kermany, Kang Zhang, and Michael Goldbaum. Labeled optical coherence tomography (oct) and chest x-ray images for classification. *Mendeley data*, 2, 2018.
- [8] Naveen Kodali, Jacob Abernethy, James Hays, and Zsolt Kira. On convergence and stability of gans. *arXiv preprint arXiv:1705.07215*, 2017.
- [9] Alex Krizhevsky, Ilya Sutskever, and Geoffrey E Hinton. Imagenet classification with deep convolutional neural networks. In *Advances in neural information processing systems*, pages 1097–1105, 2012.
- [10] Mehdi Mirza and Simon Osindero. Conditional generative adversarial nets. *arXiv preprint arXiv:1411.1784*, 2014.
- [11] Alec Radford, Luke Metz, and Soumith Chintala. Unsupervised representation learning with deep convolutional generative adversarial networks. *arXiv preprint arXiv:1511.06434*, 2015.
- [12] Olaf Ronneberger, Philipp Fischer, and Thomas Brox. U-net: Convolutional networks for biomedical image segmentation. In *International Conference on Medical image computing and computer-assisted intervention*, pages 234–241. Springer, 2015.

- [13] Tim Salimans, Ian Goodfellow, Wojciech Zaremba, Vicki Cheung, Alec Radford, and Xi Chen. Improved techniques for training gans. In *Advances in neural information processing systems*, pages 2234–2242, 2016.
- [14] Veit Sandfort, Ke Yan, Perry J Pickhardt, and Ronald M Summers. Data augmentation using generative adversarial networks (cylegan) to improve generalizability in ct segmentation tasks. *Scientific reports*, 9(1):1–9, 2019.
- [15] Thomas Schlegl, Philipp Seeböck, Sebastian M Waldstein, Ursula Schmidt-Erfurth, and Georg Langs. Unsupervised anomaly detection with generative adversarial networks to guide marker discovery. In *International conference on information processing in medical imaging*, pages 146–157. Springer, 2017.
- [16] Christian Szegedy, Vincent Vanhoucke, Sergey Ioffe, Jon Shlens, and Zbigniew Wojna. Rethinking the inception architecture for computer vision. In *Proceedings of the IEEE conference on computer vision and pattern recognition*, pages 2818–2826, 2016.
- [17] Zhou Wang, Alan C Bovik, Hamid R Sheikh, and Eero P Simoncelli. Image quality assessment: from error visibility to structural similarity. *IEEE transactions on image processing*, 13(4):600–612, 2004.
- [18] Eric Wu, Kevin Wu, David Cox, and William Lotter. Conditional infilling gans for data augmentation in mammogram classification. In *Image Analysis for Moving Organ, Breast, and Thoracic Images*, pages 98–106. Springer, 2018.
- [19] Han Zhang, Ian Goodfellow, Dimitris Metaxas, and Augustus Odena. Self-attention generative adversarial networks. *arXiv preprint arXiv:1805.08318*, 2018.
- [20] Yu-Dong Zhang, Zhengchao Dong, Xianqing Chen, Wenjuan Jia, Sidan Du, Khan Muhammad, and Shui-Hua Wang. Image based fruit category classification by 13-layer deep convolutional neural network and data augmentation. *Multimedia Tools and Applications*, 78(3):3613–3632, 2019.